Available online at www.sciencedirect.com
SCIENCE DIRECT®
Journal of Solid State Chemistry 179 (2006) 186–194
JOURNAL OF SOLID STATE CHEMISTRY
www.elsevier.com/locate/jssc

Crystal structures of alkali-metal indium (III) phosphates of $[M_3In(PO_4)_2]_n$ ($M = K$, $n = 10$; $M = Rb$, $n = 2$) compounds, and band structures and chemical bond properties of $[Rb_3In(PO_4)_2]_2$ crystal

Yongchun Zhang, Wendan Cheng*, Dongsheng Wu, Hao Zhang, Dagui Chen, Yajing Gong, Zigui Kan, Jing Zhu

Fujian Institute of Research on the Structure of Matter, Chinese Academy of Sciences, State Key Laboratory of Structural Chemistry, The Graduate School of the Chinese Academy of Sciences, Fuzhou Fujian 350002, People's Republic of China

Received 3 June 2005; received in revised form 26 July 2005; accepted 23 September 2005
Available online 28 November 2005

Abstract

Ternary indium (III) phosphates with three-dimensional frameworks, $[M_3In(PO_4)_2]_n$ ($M = K$, $n = 10$; $M = Rb$, $n = 2$), are found and firstly reported in this paper. These compounds have been obtained by high temperature solid-state reactions and their crystal structures have been determined by single crystal X-ray diffraction analysis. The title compounds, which crystallize in monoclinic system, possess the same $[In(PO_4)_2]_n^{3n-}$ anionic frameworks built up from interconnected InO_6 octahedra and PO_4 tetrahedra and have an interesting tunnel structure where M^+ cations are located. Optical and bonding properties of $[Rb_3In(PO_4)_2]_2$ are investigated in terms of measured absorption and emission spectra, and calculated band structures and density of states. The crystal band structures obtained by the DFT method show that the solid compound of $[Rb_3In(PO_4)_2]_2$ is an insulator with direct band gap, and the P–O covalent bond characters are larger than the In–O ones in this compound.

Keywords: Phosphate; Crystal structure; Band structure; DFT method

1. Introduction

Metal phosphates possessing open-framework structures with defined tunnels are extensively investigated for their structural diversity, various properties, as well as potential applications in shape-selective catalysis, absorbents, ion-exchange solids, and molecular sieves [1–3]. In addition to the well-known aluminophosphates and gallophosphates [4], a great number of new metal phosphates with open-frameworks were reported, with metals including iron [5], indium [6], titanium [7], vanadium [8], zirconium [9], and molybdenum [10]. In these compounds, the octahedral coordination of the metal centers combined with the tetrahedral geometry of the phosphate groups is the origin of a large variety of structures. Specially, there has recently been much interest in the ternary phosphates containing alkaline metals along with various other metals due to the possibility of using these compounds in single and polycrystalline form as nonlinear optical materials [11], solid electrolytes [12–14], ionic conductors [15–20], battery electrodes [21,22], sensors for detection of NOX in atmospheric environment [23], etc. Although the study of metal phosphates was conspicuous and some inspiring results were recently achieved, there is very scant information on the ternary alkali metal phosphates containing the indium atoms in the literature [24–38]. Additionally, the band structures and optical properties of these typical solid compounds have been seldom reported in contrast to the alkali metal titanyl phosphates, which are mostly investigated in this respect [39–41].

Here, we will present synthesis, crystal structure determinations, and spectrum measurements for indium phosphates $[M_3In(PO_4)_2]_n$ ($M = K$, $n = 10$; $M = Rb$, $n = 2$). At

*Corresponding author. Tel.: +86 591 379 3068; fax: +86 591 371 4946.
E-mail address: cwd@ms.fjirsm.ac.cn (W. Cheng).

0022-4596/$ - see front matter © 2005 Elsevier Inc. All rights reserved.
doi:10.1016/j.jssc.2005.09.050

the same time, we will make the calculations of crystal energy band structures in order to understand the chemical bonding properties and electronic origin of optical transition for $[Rb_3In(PO_4)_2]_2$ solid compound.

2. Experimental section

2.1. Crystal growth

The single crystals of $[K_3In(PO_4)_2]_{10}$ and $[Rb_3In(PO_4)_2]_2$ were prepared by solid state reactions among In_2O_3 (99.99%, Shanghai Chemical Company), $NH_4H_2PO_4$ and either KNO_3 or Rb_2CO_3 (Analytical Grade, Shanghai Chemical Company), in a molar ratio corresponding to $In/P/M = 1:9:15$. The samples were ground and heated in air at 923 K for 10 h and afterwards at 1273 K for 24 h in a platinum crucible. The mixtures were then cooled to 1023 K at a rate of $2\,K\,h^{-1}$ and finally quenched to room temperature. Some colorless crystals were selected carefully, but the other phases may be present in the remaing batch.

2.2. Crystal structures determination

Single crystals of $[M_3In(PO_4)_2]_n$ having the dimensions $0.32 \times 0.25 \times 0.23\,mm^3$ ($M = K$, $n = 10$) and $0.24 \times 0.16 \times 0.16\,mm^3$ ($M = Rb$, $n = 2$) were selected for intensity data which were collected on a Siemens SMART CCD diffractometer with graphite monochromated Mo$K\alpha$ radiation ($\lambda = 0.71073$ Å) at the temperature of 293 K using the scan mode. Lorentz and polarization corrections were applied to the data. The structures of $[M_3In(PO_4)_2]_n$ ($M = K$, $n = 10$; $M = Rb$, $n = 2$) were solved by direct method and then refined on F^2 by full-matrix least-squares method, and performed in the Shelxl/PC programs. Crystal structure data for these compounds are summarized in Table 1 and the atomic coordinates and thermal parameters are listed in Table 2.

2.3. Spectrum measurements

The samples used for spectrum measurements were prepared from pressed abradant of selected micro-crystals due to the fact that we have not successfully synthesized the compounds at the correct composition as monophasic powder samples. In order to give an evidence that it contains pure phase of samples, we determine the powder XRD pattern of $[Rb_3In(PO_4)_2]_2$ using X'Pert diffractometer with a monochromated Cu$K\alpha$ X-ray source (step size of 0.02° and range $2\theta = 10-85°$). Fig. 1(a) gives the powder X-ray diffraction pattern of $[Rb_3In(PO_4)_2]_2$. Comparing Fig. 1(a) with Fig. 1(b), we can find that the peak positions are from $2\theta = 20°$ to $2\theta = 56°$, and the two strongest peaks localized about $2\theta = 30°$ are overlap well. Accordingly, this pattern compares with that simulated by the program Visualizer Software using the crystallographic data, confirming the monophasic nature of the prepared samples. The absorption spectra were recorded by a Cary-500 UV–VIS–NIR Spectrophotometer at 300 K from 200 to 1500 nm, and the luminescence were measured by FL/FS

Table 1
Crystal data and structure refinement parameters for the title compounds

Empirical formula	$[K_3In(PO_4)_2]_{10}$	$[Rb_3In(PO_4)_2]_2$
Formula weight	4220.6	1122.34
T (K)	293(2)	293(2)
Wavelength (Å)	0.71073	0.71073
Crystal system	Monoclinic	Monoclinic
Space group	$C2/c$	$P2(1)/n$
a (Å)	42.0671(4)	9.9827(1)
b (Å)	11.2166(2)	11.6358(2)
c (Å)	18.5081(1)	15.9307(3)
β (°)	100.15	90.27
V (Å^3)	8596.4(2)	1850.4(1)
Z	4	4
Calculated density ($g\,cm^{-3}$)	3.261	4.029
Absorption coefficient (mm^{-1})	4.588	18.595
$F(000)$	8000	2032
Crystal size (mm)	$0.32 \times 0.25 \times 0.23$	$0.24 \times 0.16 \times 0.16$
θ range for data collection (°)	0.98–25.01	2.17–26.06
Index ranges	$-49 \leqslant h \leqslant 39$, $-7 \leqslant k \leqslant 13$, $-21 \leqslant l \leqslant 21$	$-12 \leqslant h \leqslant 11$, $-13 \leqslant k \leqslant 14$, $-19 \leqslant l \leqslant 19$
Reflections collected	13594	12143
Reflections unique	7491 (Rint = 0.0243)	3667 (Rint = 0.0526)
Parameter/restraints/data (obs.)	642/0/6815	254/0/3151
Goodness-of-fit on F^2	1.142	1.212
Final R indices [$I > 2\sigma(I)$]	$R_1 = 0.0412$, $\omega R_2 = 0.1054$	$R_1 = 0.0435$, $\omega R_2 = 0.0877$
R indices (all data)	$R_1 = 0.0460$, $\omega R_2 = 0.1115$	$R_1 = 0.0569$, $\omega R_2 = 0.0914$
Largest difference peak and hole ($e\,A^{-3}$)	1.101, −2.668	2.093, −1.380

Table 2
Fractional atomic coordinates and equivalent isotropic displacement parameters[a] of $[K_3In(PO_4)_2]_{10}$ and $[Rb_3In(PO_4)_2]_2$

Atom	x	y	z	U_{eq}[b]
(a) $[K_3In(PO_4)_2]_{10}$				
In1	0.212584(9)	0.60245(3)	0.92480(2)	0.01014(12)
In2	0.193148(9)	0.38127(3)	0.68989(2)	0.00988(12)
In3	0.012875(9)	0.39280(3)	0.61493(2)	0.01037(12)
In4	0.105678(9)	0.86583(4)	0.01096(2)	0.01113(12)
In5	0.087857(9)	0.09698(4)	0.78233(2)	0.01218(13)
K1	0.19480(3)	0.14763(13)	0.55178(7)	0.0195(3)
K2	0.0000	0.85356(17)	0.2500	0.0185(4)
K3	0.03608(3)	0.89733(13)	0.44922(8)	0.0216(3)
K4	0.24041(3)	0.12431(13)	0.75346(8)	0.0255(3)
K5	0.10743(4)	0.12843(13)	0.14520(8)	0.0237(3)
K6	0.14423(3)	0.35038(13)	0.85408(7)	0.0215(3)
K7	0.15939(3)	0.14744(12)	0.34361(7)	0.0209(3)
K8	0.10277(3)	0.37658(13)	0.64002(7)	0.0201(3)
K9	0.21550(4)	0.13206(13)	0.95122(8)	0.0261(3)
K10	0.19096(3)	0.36344(12)	0.05078(7)	0.0200(3)
K11	0.94240(3)	0.61438(12)	0.57173(8)	0.0213(3)
K12	0.0000	0.60583(16)	0.7500	0.0165(4)
K13	0.09301(3)	0.32559(13)	0.97208(8)	0.0255(3)
K14	0.90956(4)	0.62958(13)	0.75671(9)	0.0279(3)
K15	0.01567(4)	0.85299(13)	0.65025(8)	0.0279(3)
K16	0.20202(6)	0.8566(2)	0.70833(16)	0.0354(5)
K17	0.1900(2)	0.8603(8)	0.6616(6)	0.037(2)
P1	0.23717(3)	0.39071(13)	0.87084(8)	0.0096(3)
P2	0.25447(3)	0.62238(12)	0.09848(8)	0.0089(3)
P3	0.94518(3)	0.38132(13)	0.70595(8)	0.0093(3)
P4	0.06365(3)	0.87627(13)	0.82957(8)	0.0104(3)
P5	0.14694(3)	0.60454(13)	0.00606(8)	0.0099(3)
P6	0.17210(3)	0.60091(13)	0.73951(8)	0.0106(3)
P7	0.14872(3)	0.12788(13)	0.69674(8)	0.0105(3)
P8	0.03526(3)	0.60835(12)	0.55937(8)	0.0107(3)
P9	0.04522(3)	0.11830(13)	0.60571(8)	0.0105(3)
P10	0.13067(3)	0.08162(13)	0.96305(8)	0.0116(3)
O1	0.27469(10)	0.7162(4)	0.0662(2)	0.0186(9)
O2	0.17064(10)	0.6607(4)	0.9608(3)	0.0242(10)
O3	0.23024(9)	0.6889(4)	0.1384(2)	0.0162(8)
O4	0.20633(9)	0.4040(4)	0.9061(2)	0.0145(8)
O5	0.00727(10)	0.5990(4)	0.6035(2)	0.0168(9)
O6	0.19845(10)	0.5773(4)	0.6909(2)	0.0151(8)
O7	0.04787(9)	0.4772(4)	0.5578(2)	0.0142(8)
O8	0.10157(10)	0.0646(4)	0.0046(2)	0.0168(9)
O9	0.11650(9)	0.6838(4)	0.9968(2)	0.0162(8)
O10	0.95038(9)	0.4230(4)	0.7877(2)	0.0171(9)
O11	0.15591(9)	0.4761(4)	0.7415(2)	0.0163(9)
O12	0.09433(10)	0.9004(4)	0.7956(2)	0.0170(9)
O13	0.14839(10)	0.6971(4)	0.7074(2)	0.0212(9)
O14	0.25386(9)	0.5153(4)	0.8837(2)	0.0175(9)
O15	0.17938(9)	0.2062(4)	0.7127(2)	0.0208(9)
O16	0.04382(10)	0.7735(4)	0.7906(2)	0.0213(9)
O17	0.97610(10)	0.4112(4)	0.6758(2)	0.0241(10)
O18	0.23567(10)	0.5493(4)	0.0335(2)	0.0171(9)
O19	0.06290(10)	0.0550(4)	0.6759(2)	0.0216(9)
O20	0.22920(10)	0.3670(4)	0.7879(2)	0.0200(9)
O21	0.02334(10)	0.6491(4)	0.4794(2)	0.0183(9)
O22	0.02079(9)	0.2100(3)	0.6282(2)	0.0153(8)
O23	0.07176(10)	0.8475(4)	0.9115(2)	0.0217(10)
O24	0.06908(10)	0.1887(4)	0.5681(2)	0.0183(9)
O25	0.14396(9)	0.9520(4)	0.9602(2)	0.0157(8)
O26	0.12252(9)	0.1896(4)	0.7333(2)	0.0182(9)
O27	0.11802(11)	0.1300(4)	0.8859(2)	0.0237(10)
O28	0.27620(10)	0.5393(4)	0.1499(2)	0.0199(9)
O29	0.13819(10)	0.4787(4)	0.9812(3)	0.0243(10)
O30	0.06171(10)	0.6935(4)	0.5952(2)	0.0201(9)
O31	0.02690(10)	0.0235(4)	0.5578(2)	0.0228(10)
O32	0.18932(12)	0.6414(4)	0.8152(2)	0.0244(10)
O33	0.16206(11)	0.6051(4)	0.0879(2)	0.0249(10)
O34	0.13787(11)	0.1220(4)	0.6135(2)	0.0232(10)
O35	0.94044(10)	0.2465(4)	0.6993(2)	0.0245(10)
O36	0.91689(10)	0.4478(4)	0.6633(2)	0.0248(10)
O37	0.04498(10)	0.9952(4)	0.8204(2)	0.0225(9)
O38	0.15571(10)	0.0038(4)	0.7273(2)	0.0236(10)
O39	0.15582(11)	0.1673(4)	0.0012(3)	0.0292(11)
O40	0.25917(10)	0.2913(4)	0.9067(2)	0.0206(9)
(b) $[Rb_3In(PO_4)_2]_2$				
In1	0.07769(8)	0.86903(7)	0.86885(5)	0.0082(2)
In2	0.57347(8)	0.15252(7)	0.88588(5)	0.0083(2)
Rb1	0.18742(13)	0.13607(11)	0.75724(8)	0.0202(3)
Rb2	0.23967(12)	0.10696(11)	0.00078(8)	0.0177(3)
Rb3	0.20595(14)	0.61980(10)	0.00778(8)	0.0189(3)
Rb4	0.89957(13)	0.12162(11)	0.58370(9)	0.0237(3)
Rb5	0.71115(13)	0.90112(11)	0.75350(8)	0.0197(3)
Rb6	0.38629(13)	0.91604(11)	0.67215(9)	0.0250(4)
P1	0.0646(3)	0.8621(3)	0.64526(18)	0.0089(6)
P2	0.0811(3)	0.3787(2)	0.60146(18)	0.0074(6)
P3	0.9439(3)	0.6586(2)	0.83733(18)	0.0087(6)
P4	0.9147(3)	0.1336(2)	0.90596(18)	0.0066(6)
O1	0.0982(8)	0.6798(7)	0.8529(5)	0.0130(18)
O2	0.2240(9)	0.4257(8)	0.6202(6)	0.023(2)
O3	0.0775(9)	0.3113(7)	0.5193(5)	0.0159(19)
O4	0.0348(9)	0.3006(7)	0.6721(5)	0.0167(19)
O5	0.9239(10)	0.6195(8)	0.7467(6)	0.024(2)
O6	0.8820(9)	0.7793(7)	0.8553(6)	0.0177(19)
O7	0.9123(8)	0.8441(7)	0.6327(5)	0.0143(18)
O8	0.8902(10)	0.5652(8)	0.8939(5)	0.021(2)
O9	0.0092(9)	0.0385(7)	0.8729(6)	0.021(2)
O10	0.1211(9)	0.9560(7)	0.5879(5)	0.019(2)
O11	0.9871(9)	0.4829(8)	0.5943(6)	0.022(2)
O12	0.7690(9)	0.0908(8)	0.8901(6)	0.022(2)
O13	0.9412(10)	0.2452(8)	0.8596(6)	0.023(2)
O14	0.1258(9)	0.7418(7)	0.6224(6)	0.020(2)
O15	0.1020(11)	0.8932(8)	0.7360(6)	0.025(2)
O16	0.9394(11)	0.1501(9)	0.0002(6)	0.029(2)

[a]The positions of K(16) and K(17) are disorder and give a statistical distribution, K(16) has 80% and K(17) has 20%. K(2) and K(12) are the special position.
[b]$U_{eq} = (1/3)\sum_i\sum_j U_{ij}a_i * a_j * a_i a_j$.

900 Time Resolved Fluorescence Spectrometer using Xe lamp at room temperature.

2.4. Computational descriptions

The crystallographic data of the ternary indium (III) phosphate $[Rb_3In(PO_4)_2]_2$ determined by X-ray were used to calculate electronic band structures of the solid states. The calculations of band structures were made by the density functional theory (DFT) with the nonlocal gradient-corrected exchange-correlation functional [42] and performed with the CASTEP code [43,44], which uses a plane wave basis set for the valence electrons and

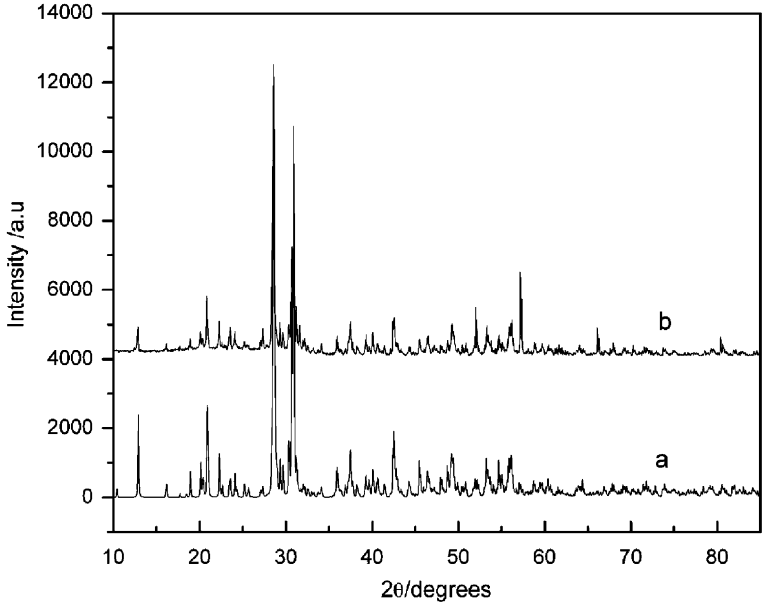

Fig. 1. Simulated (a) and experimental (b) powder X-ray (Cu$K\alpha$) diffraction patterns for $[Rb_3In(PO_4)_2]_2$

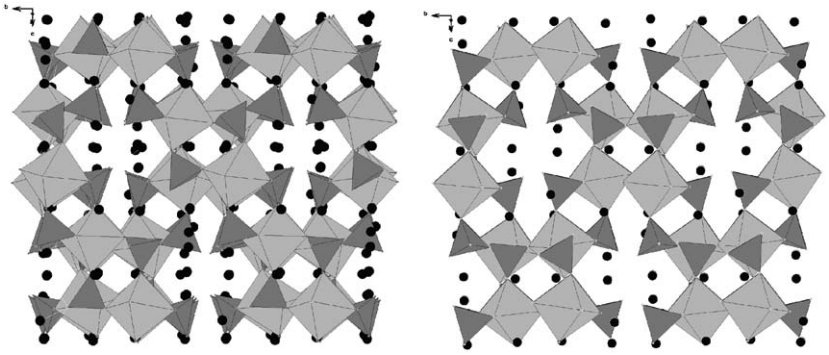

Fig. 2. Crystal structures along [001], left (a) for $[K_3In(PO_4)_2]_{10}$ and right (b) for $[Rb_3In(PO_4)_2]_2$: indium octahedra are light gray; phosphorus tetrahedra are medium gray; potassium or rubidium cations are represented by black circles.

norm-conserving pseudopotential [45] for the core states. The number of plane waves included in the basis was determined by a cutoff energy of 450 eV. Pseudo-atomic calculations were performed for O $2s^2 2p^4$, P $3s^2 3p^3$, In $5s^2 5p^1$, and Rb $4s^2 4p^6 5s^1$. The calculating parameters and convergent criterions were set by the default values of CASTEP code [43]. The calculations of linear optical properties described in terms of the complex dielectric function $\varepsilon = \varepsilon_1 + i\varepsilon_2$ were also made in this work. The imaginary part of the dielectric functions $\varepsilon(\omega)_2$ is given by [46]

$$\varepsilon_2(\omega) = 4(\pi e/m\omega)2\sum_{v,c}\int_{BZ} 2\,\mathrm{d}k/(2\pi)^3 \times \left|e.\mathrm{Mcv}(k)\right|\delta(\mathrm{Ec}(K) - \mathrm{Ev}(K) - \hbar\omega). \quad (1)$$

CASTEP calculates the real $\varepsilon(\omega)_1$ and imaginary $\varepsilon(\omega)_2$ parts of the dielectric function [43]. The $\varepsilon(\omega)_2$ be thought of as detailing the real transitions between occupied and unoccupied electronic states. The real and imaginary parts are linked by a Kramers–Kronig transform [46]. This transform is used to obtain the real part $\varepsilon(\omega)_1$ of the dielectric function.

3. Result and discussion

3.1. Crystal structures of $[M_3In(PO_4)_2]_n$ ($M = K$, $n = 10$; $M = Rb$, $n = 2$)

As shown in Fig. 2, the compounds $[M_3In(PO_4)_2]_n$ ($M = K$, $n = 10$; $M = Rb$, $n = 2$) possess three-dimensional $[In(PO_4)_2]_n^{3n-}$ anionic frameworks that build up from $[InO_6]$ octahedra and $[PO_4]$ tetrahedra. Some of M^+ ions ($M = K$, Rb) locate in infinite large channels running along [001] with 8-sided windows, each window is formed by the edges of four $[InO_6]$ octahedra and four $[PO_4]$ tetrahedra. Lateral smaller 4-sided windows resulted from the edges of four $[InO_6]$ octahedra, are also observed, which are occupied by remaining M^+ cations ($M = K$, Rb). In spite of the $[In(PO_4)_2]$ framework is the same for

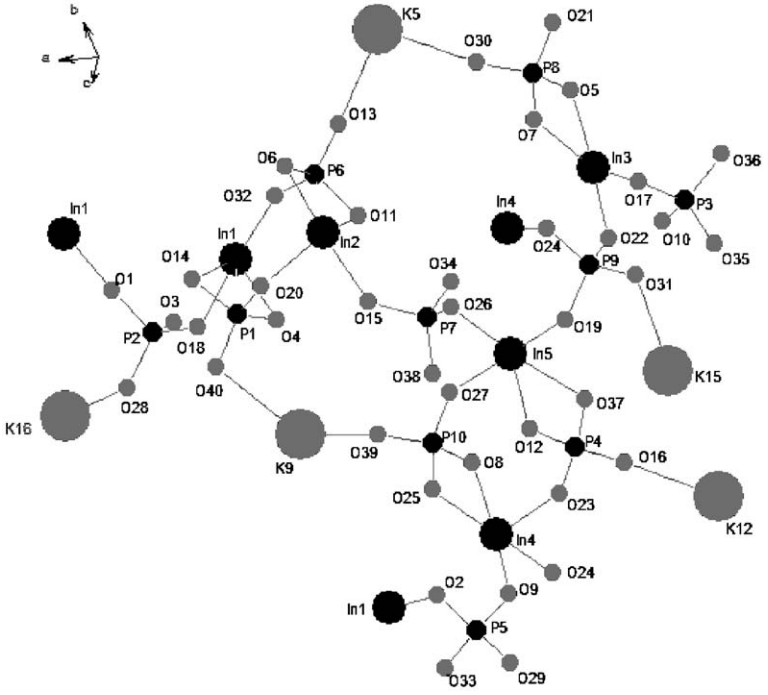

Fig. 3. A perspective view of the $[K_3In(PO_4)_2]_{10}$ structure showing the coordination of PO_4 ligands around In atoms.

the two compounds, there are more K^+ ions locate in 8- and 4-sided holes in $[K_3In(PO_4)_2]_{10}$ and the ion arrangements in the holes are the differences between the two compounds (found in Figs. 2(a) and (b)). It may be a reason that they present rather different cell parameters and different space groups for the two compounds. Now, we discuss the structures by taking $[K_3In(PO_4)_2]_{10}$ as an example. A perspective view of the $[K_3In(PO_4)_2]_{10}$ structure showing the coordination of $[PO_4]$ ligands around In atoms is illustrated in Fig. 3. Two chemically and crystallographically distinct P atoms are present in the structure: P(**I**) (P(1), P(4), P(6), P(8), P(10)) and P(**II**) (P(2), P(3), P(5), P(7), P(9)). In case of $[P(\mathbf{I})O_4]$ tetrahedron, it shares an edge with $[InO_6]$ octahedron with the third corner being connected to another $[InO_6]$ octahedron and the fourth being directed towards the channel. For $[P(\mathbf{II})O_4]$ tetrahedron, three corners of it connect three different $[InO_6]$ octahedra and the fourth connects the K^+ ions. Each $[InO_6]$ octahedron shares a common edge with P(I) tetrahedron, the other four corners with one $[P(\mathbf{I})O_4]$ tetrahedron and three different $[P(\mathbf{II})O_4]$ tetrahedra. These $[InO_6]$ octahedra are connected by $[P(\mathbf{II})O_4]$ tetrahedra to form a column along [001], which is linked to adjacent columns by $[P(\mathbf{I})O_4]$ tetrahedra so that a three-dimensional open framework structure enclosing a large channel with windows of 8-membered rings is formed.

The $[InO_6]$ octahedra are greatly distorted because of edge-sharing. The In–O distances range from 2.078(4) to 2.345(4) Å and O–In–O bond angles range from 64.60(16) to 116.86(16)°. Similarly, the $[P(\mathbf{I})O_4]$ tetrahedra are also distorted as indicated by the P(**I**)–O distances {1.505(4)–1.568(5) Å} and O–P(**I**)–O angles {102.6(2)–113.2(3)°}. The In–O and P(**I**)–O bonds involving the edge-sharing oxygen are the longest. The phosphorus atoms in the $[P(\mathbf{II})O_4]$ tetrahedra connected oxygen atoms, which connect In atoms, form three long P(**II**)–O bonds of 1.527(5)–1.562(4) Å, and one shorter bond of 1.505(4)–1.518(4) Å is formed with oxygen atoms which co-ordinate to K^+ ions. The coordination numbers (CN) of each M^+ ion were determined on the basis of the maximum gap in the M–O distances. In $[K_3In(PO_4)_2]_{10}$, the K^+ cations show from CN = 6 to CN = 10 with K–O distances ranging from 2.5424(4) to 3.4225(5) Å, in which K(9) CN = 6; K(3), K(5), K(6), K(10), K(14), K(15), CN = 7; K(1), K(7), K(8), K(11), K(12), K(13), K(16), CN = 8; K(4) CN = 9, K(2) CN = 10. In $[Rb_3In(PO_4)_2]_2$, the Rb^+ cations exhibit CN from 7 to 10 {Rb–O distances: 2.6874(8)–3.6086(7) Å}, in which Rb(2), Rb(5), CN = 7; Rb(3), Rb(4), CN = 8; Rb(6) CN = 9; Rb(1) CN = 10.

3.2. Band structure, density of states and chemical bond

The calculated band structure of $[Rb_3In(PO_4)_2]_2$ at the Brillouin zone is plotted in Fig. 4(a). It is observed that the valence bands are very flat, and the conduction bands have some oscillating. In order to make clear inspection, we plot the top seven valence bands and five conduction bands in Fig. 4(b). The lowest energy of conduction band is localized at G point, and the $[Rb_3In(PO_4)_2]_2$ shows an isolator with direct band gap of 3.18 eV.The bands can be assigned according to total and partial densities of states (DOS), as plotted in Fig. 5. The valence bands lying about between −25.0 and −22.5 eV, and between about −10.0 and −7.5 eV are almost contributions from

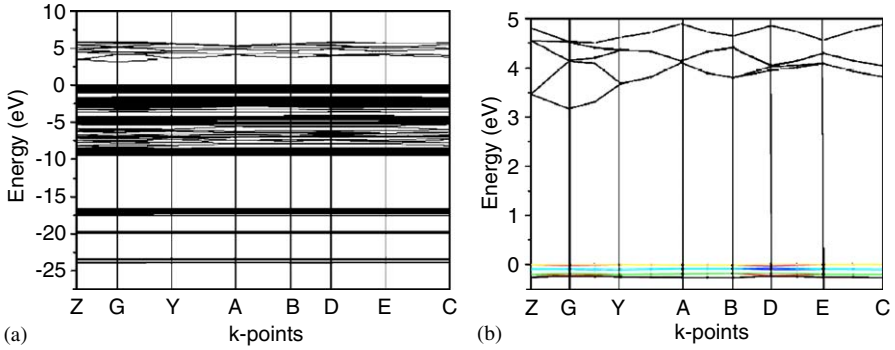

Fig. 4. The calculated band structure of $[Rb_3In(PO_4)_2]_2$ crystal.

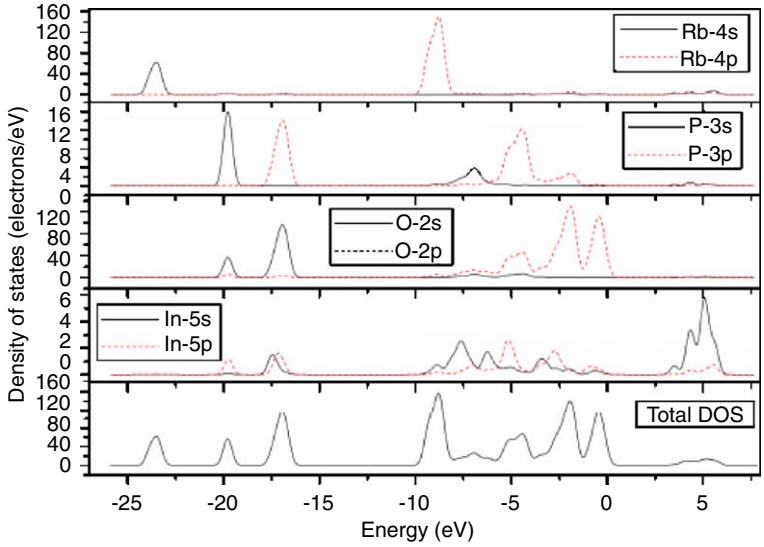

Fig. 5. The calculated total and partial density of states of. $[Rb_3In(PO_4)_2]_2$ crystal.

the Rb-4*s* and -4*p* states, respectively. The valence bands localized at about −20.0 eV are mostly contributions from the O-2*s* and P-3*s* states but with small mixings of In-5*p* states. The O-2*s* and P-3*p* states have the significant contributions to the valence bands lying about between −18.0 and −16.0 eV. The valence bands lying about between −7.5 eV and the Fermi level (0.0 eV) are most contributions from the O-2*p* and P-3*p* states but with small mixings of In-5*p* states. The band of the nearest Fermi level mostly originates from the O-2*p* states. The conduction bands localized between 3.2 and 6.0 eV are the main contributions from the In-5*s* states. The calculated band gap (3.18 eV) is as compared with the experimental value of 3.10 eV.

Now, we elucidate the feature of chemical bond from the nature of total and angular momentum projected DOS. Comparing the total DOS with the angular momentum projected DOS of P-3*p* and O-2*p* states in Fig. 5, it is seen from about −6.0 to 0.0 eV that the DOS is higher for O-2*p* states (the largest DOS of 130 electrons/eV) than P-3*p* states (the largest DOS of 12 electrons/eV), and than In-5*p* states (the largest DOS of 2.5 electrons/eV), respectively. It means that some electrons from P-3*p* and In-5*p* transform into the valence bands and take part in the covalence interactions between P or In and O atoms, but the covalence strengths are stronger between P and O than between In and O atoms. It is also found that the peaks of total DOS around −23.0 and −8.0 eV completely attribute to Rb-5*s* and -5*p* states. This implies that there are pure ionic bonds between Rb and O atoms. The chemical bond properties are also evidences from the population analysis. The calculated bond orders between P and O atoms are from 0.60 to 0.78 e, between In and O atoms are from 0.25 to 0.43 e, and between Rb and O atoms are from 0.00 to 0.17 e in a unit cell of $[Rb_3In(PO_4)_2]_2$ (pure covalence single bond order is generally 1.0 e). Accordingly, we can also say that the covalence strength is stronger for the P–O bond than the In–O bond, and ionic strength is stronger for the Rb–O bond than the In–O bond in $[Rb_3In(PO_4)_2]_2$.

3.3. Optical properties of $[Rb_3In(PO_4)_2]_2$

Fig. 6(a) shows the absorption spectra of $[Rb_3In(PO_4)_2]_2$ powder determined from reflection measurements by UV–Vis DRIS. It is seen that the absorption edge is at about 400 nm (3.10 eV) and first absorption peak (shoulder

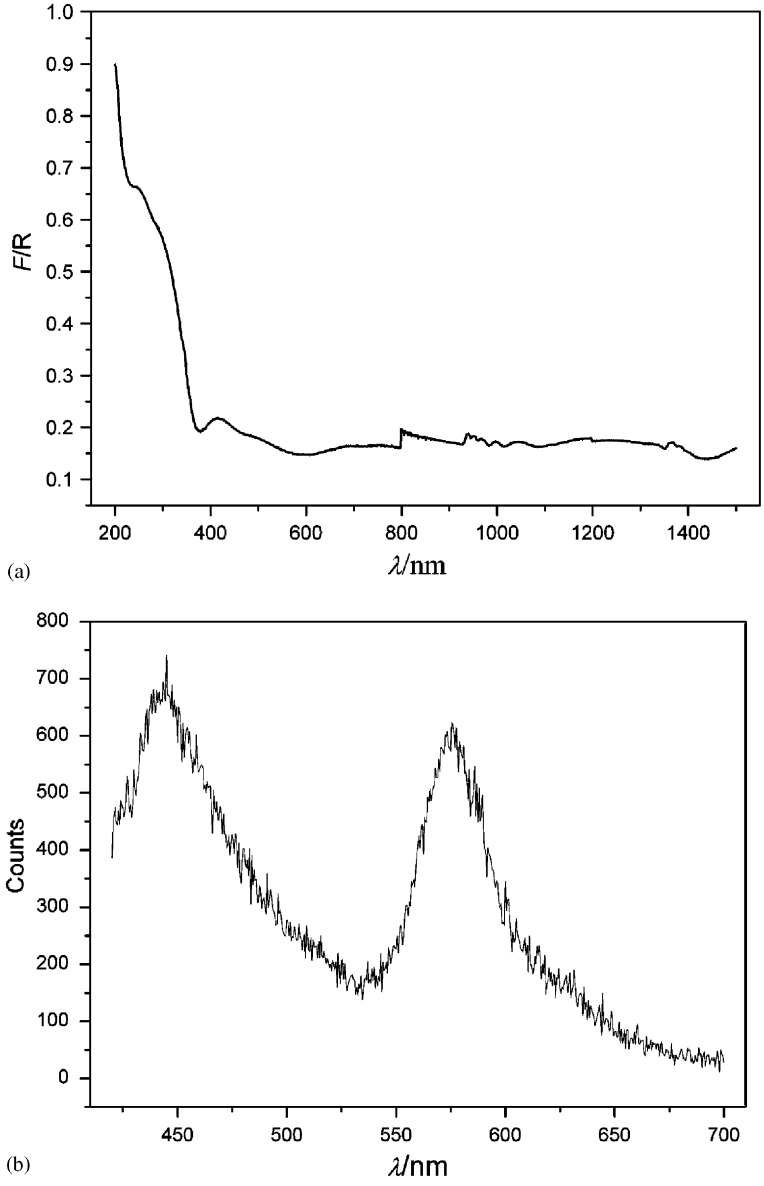

Fig. 6. Observed (a) absorption and (b) emission spectra of $[Rb_3In(PO_4)_2]_2$.

peak) is at about 220 nm (5.64 eV). According to the early analysis of band structures, we assign these absorption edge and peak as the electron transitions from the O-2*p* to the In unoccupied atomic states. Wide transmission ranges from about 400 to 1500 nm for $[Rb_3In(PO_4)_2]_2$ were also observed. Fig. 6(b) shows that two emission peaks are located at 445 and 575 nm when a light of 355 nm is incidence on the powder sample of $[Rb_3In(PO_4)_2]_2$. Comparing the absorption edge with the observed emitted peak, we can deduce that the emitted fluorescence originates from defects or excitons due to the fact of that emission wavelength of 445 nm is larger than the optical absorption edge of 400 nm. It is reported that the absorption edge and shoulder peak are at 400 and 250 nm, and emission peaks are at 522 and 622 nm for the $RbInP_2O_7$ powder [47]. By comparison between the spectra of $[Rb_3In(PO_4)_2]_2$ and those of $RbInP_2O_7$, we find that the absorption peak (shoulder) and emitted peaks of former have the blue shifts of tens of nm.

The calculated imaginary $\varepsilon_2(\omega)$ and the real $\varepsilon_1(\omega)$ parts of the frequency-dependent dielectric functions without the scissor-operator approximation are displayed in Fig. 7. The part $\varepsilon_2(\omega)$ can be used to describe the real transitions between occupied and unoccupied electronic states. It is found from the dispersion of the calculated $\varepsilon_2(\omega)$ spectra that there are the first absorption peaks localized at about 7.31 eV (170 nm), and 6.51 eV (190 nm), in x (or y), z polarization directions for $[Rb_3In(PO_4)_2]_2$ crystal, respectively. The crystal is transparent while the wavelength is larger than 376 nm or photon energy is less than 3.30 eV. Comparing them with the observed absorption edge (3.10 eV) and shoulder peak (5.64 eV) of powder

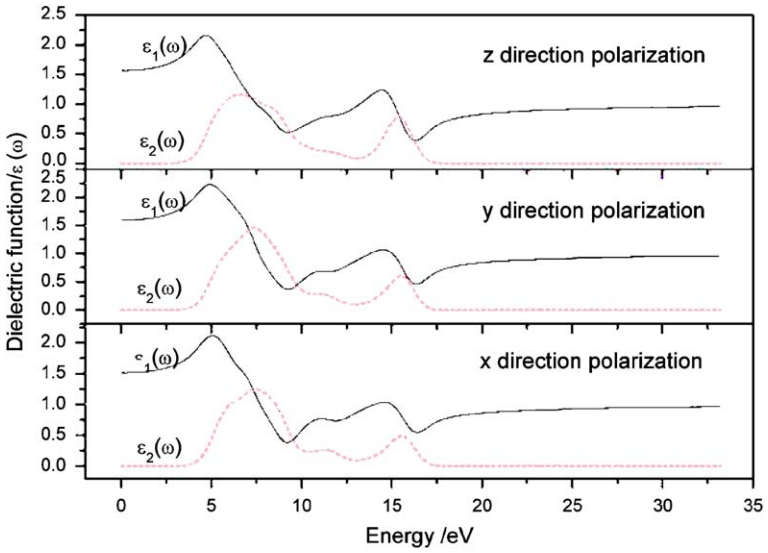

Fig. 7. The calculated dielectric functions based on DFT band structures.

$[Rb_3In(PO_4)_2]_2$, we find that the absorption band from 3.1 to 6.0 eV originates from charge transfers from O-2*p* to In-5*s* states in view of analysis of the calculated DOS, which shows that the conduction bands localized between 3.2 and 6.0 eV are main the contributions from the In-5*s* states and top valence bands are formed from the O-2*p* states. From the real $\varepsilon_1(\omega)$ parts of Fig. 7, we also find that the calculated dielectric constant of static case, $\varepsilon(0)$, i.e. $\varepsilon_1(\omega \to 0)$, is about 1.5102, 1.5914, and 1.5657 in *x*, *y*, and *z* directions for $[Rb_3In(PO_4)_2]_2$ crystal, respectively.

4. Conclusion

In the present work, $[M_3In(PO_4)_2]_n$ ($M = K$, $n = 10$; $M = Rb$, $n = 2$) have been synthesized by solid-state reaction and their structures have been determined by the single crystal X-ray diffraction technique. These compounds possess the same three-dimensional $[In(PO_4)_2]_n^{3n-}$ anionic frameworks with channels occupied by M^+ ions. The frameworks are built up from interconnected $[InO_6]$ octahedra and $[PO_4]$ tetrahedra. The observed absorption edge and shoulder peak is separate at about 400 and 220 nm, and two emission peaks are located at 445 nm and 575 nm for the powder phase of $[Rb_3In(PO_4)_2]_2$. The calculated band structures show that the solid state of $[Rb_3In(PO_4)_2]_2$ is an insulator with direct band gap at about 3.18 eV and the optical transition of lowest energy mainly originates from O-2*p* to In-5*s* states. In $[Rb_3In(PO_4)_2]_2$, the $[PO_4]$ tetrahedra have covalence bond characters and the Rb–O ionic interactions are stronger. The optical dielectric constant of $[Rb_3In(PO_4)_2]_2$ crystal is estimated to be 1.5102, 1.5914, and 1.5657 in *x*, *y*, and *z* directions, respectively, taken as theoretical predictions.

Acknowledgments

This investigation was based on work supported by the National Natural Science Foundation of China under projects 90201015 and 20373073, the Science Foundation of the Fujian Province (No.E0210028), and the Foundation of State Key Laboratory of Structural Chemistry (No. 030060).

References

[1] G. Cao, H.-G. Hong, T.E. Mallouk, Acc. Chem. Res. 25 (1992) 420–427.
[2] G. Centi, F. Trifiro, J.R. Ebner, V.M. Franchetti, Chem. Rev. 88 (1988) 55–80.
[3] A. Clearfield, Chem. Rev. 88 (1988) 125–148.
[4] A.K. Cheetham, G. Férey, T. Loiseau, Angew. Chem. Int. Ed. 38 (1999) 3269–3292.
[5] K.-H. Lii, Y. Huang, V. Zima, C. Huang, H. Lin, Y. Jiang, F. Liao, S. Wang, Chem. Mater. 10 (1998) 2599–2609.
[6] S.S. Dhingra, R.C. Haushalter, J. Chem. Soc., Chem. Commun. 21 (1993) 1665–1667.
[7] Y.-L. Liu, Z. Shi, L.-R. Zhang, Y.-L. Fu, J.-S. Chen, B.-Z. Li, J. Hua, W.-Q. Pang., Chem. Mater. 13 (2001) 2017–2022.
[8] Z. Bircask, W.T.A. Harrison, Inorg. Chem. 37 (1998) 3204–3208.
[9] D. Wang, R.B. Yu, N. Kumada, N. Kinomura, Chem. Matter. 12 (2000) 956–960.
[10] R.C. Haushalter, L.A. Mundi, Chem. Mater. 4 (1992) 31–48.
[11] M.E. Hagerman, K.R. Poeppelmeier, Chem. Mater. 7 (1995) 602–621.
[12] H. Aono, E. Sugimoto, Y. Sadaoka, N. Imanaka, G. Adachi, J. Electrochem. Soc. 140 (1993) 1827–1833.
[13] H. Aono, E. Sugimoto, Y. Sadaoka, N. Imanaka, G. Adachi, Solid State Ionics 62 (1993) 309–316.
[14] A.K. Ivanov-Schitz, A.V. Nistuk, N.G. Chaban, Solid State Ionics 139 (2001) 153–157.
[15] J.P. Boilot, G. Collin, P. Colomban, J. Solid State Chem. 73 (1988) 160–171.

[16] H. Aono, E. Sugimoto, Y. Sadaoka, N. Imanaka, G. Adachi, Chem. Lett. 12 (1993) 2033–2036.
[17] F. Sanz, C. Parada, J.M. Rojo, C. Ruiz-Valero, R. Saez-Puche, J. Solid State Chem. 145 (1999) 604–611.
[18] N. Dridi, A. Boukhari, J.M. Réau, E. Arbib, E.M. Holt, Solid State Ionics 127 (2000) 141–149.
[19] A. Laghzizil, P. Barboux, A. Bouhaouss, Solid State Ionics 128 (2000) 177–181.
[20] M. Catti, S. Stramare, Solid State Ionics 136–137 (2000) 489–494.
[21] C. Delmas, A. Nadiri, J.L. Soubeyroux, Solid State Ionics 28–30 (1988) 419–423.
[22] A. Yamada, S.C. Chung, K. Hinokuma, J. Electrochem. Soc. 148 (2001) A224–A229.
[23] M. Ono, K. Shimanoe, N. Miura, N. Yamazoe, Solid State Ionics 136–137 (2000) 583–588.
[24] D. Tran Qui, S. Hamdoune, Y. Le Page, Acta Crystallogr. Sect. C 43 (1987) 201–202.
[25] D. Tran Qui, S. Hamdoune, Acta Crystallogr. Sect. C 43 (1987) 397–399.
[26] E.A. Genkina, L.A. Muradyan, B.A. Maksimov, B.V. Merinov, S.E. Sigarev, Kristallografiya 32 (1987) 74–78.
[27] K.-H. Lii, Eur. J. Solid State Inorg. Chem. 33 (1996) 519–526.
[28] M.G. Zhizhin, L.N. Komissarova, B.I. Lazoryak, F.M. Spiridonov, Doklady Akad. Nauk 365 (1999) 61–63.
[29] M.G. Zhizhin, V.A. Morozov, A.P. Bobylev, A.M. Popov, et al., J. Solid State Chem. 149 (2000) 99–106.
[30] K.-H. Lii, J. Ye, J. Solid State Chem. 131 (1997) 131–137.
[31] P.G. Nagornyi, Dopov. Nats. Akad. Nauk. Ukr. (1998) 141–146.
[32] N.V. Stus, V.V. Lisnyak, P.G. Nagornyi, J. Alloys Compd. 314 (2001) 62–66.
[33] M.P. Attfield, A.K. Cheetham, S. Natarajan, Mater. Res. Bull. 35 (2000) 1007–1015.
[34] J.-X. Mi, Y.-X. Huang, S.-Y. Mao, X.-D. Huang, Z.-B. Wei, Z.-L. Huang, J.-T. Zhao, J. Solid State Chem. 157 (2001) 213–219.
[35] K.-H. Lii, J. Chem. Soc. Dalton Trans. 6 (1996) 815–818.
[36] S.S. Dhingra, R.C. Haushalter, J. Solid State Chem. 112 (1994) 96–99.
[37] E.V. Murashova, N.N. Chudinova, Inorg. Mater. 37 (2001) 1298–1301.
[38] A.V. Arakcheeva, G. Chapuis, V. Petricek, M. Dusek, A. Schoenleber, Acta. Crystallogr. B 59 (2003) 17–27.
[39] W.Y. Ching, Y.-N. Xu, Phys. Rev. B 44 (1991) 5332–5335.
[40] F.C. Zumsteg, J.D. Bierlein, T.E. Gier, J. Appl. Phys. 47 (1976) 4980–4985.
[41] M.L. Phillips, T.E. Gier, M.M. Eddy, N.L. Keder, G.D. Stucky, J.D. Bierlein, Solid State Ionics 32–33 (1989) 147–153.
[42] J.P. Perdew, K. Burke, M. Ernzerhof, Phys. Rev. Lett. 77 (1996) 3865–3868.
[43] M. Segall, P. Lindan, M. Probert, C. Pickard, P. Hasnip, S. Clark, M. Payne, Materials Studio CASTEP, version 2.2, 2002.
[44] M.D. Segall., P.L.D. Lindan, M.J. Probert, C.J. Pickard, P.J. Hasnip, S.J. Clark, M.C. Payne, J. Phys.: Cond. Matter 14 (2002) 2717–2744.
[45] D.R. Hamann, M. Schluter, C. Chiang, Phys. Rev. Lett. 43 (1979) 1494–1497.
[46] F. Bassani, G.P. Parravicini, Electronic States and Optical Transitions In Solids, Pergamon Press Ltd., Oxford, 1975, pp. 149–154.
[47] Y.-C. Zhang, W.-D. Cheng, D.-S. Wu, H. Zhang, D.-G. Chen, Y.-J. Gong, Z.-G. Kan, Chem. Mater. 16 (2004) 4150–4159.